LASER INTERFEROMETER GRAVITATIONAL WAVE OBSERVATORY
- LIGO -
CALIFORNIA INSTITUTE OF TECHNOLOGY
MASSACHUSETTS INSTITUTE OF TECHNOLOGY

Technical Note **LIGO-T970084-00 - D** 2/26/97

Frequency Response of the LIGO Interferometer

ISC group,
Daniel Sigg, ed.

Distribution of this draft:

ISC

This is an internal working note
of the LIGO Project.

California Institute of Technology
LIGO Project - MS 51-33
Pasadena CA 91125
Phone (818) 395-2129
Fax (818) 304-9834
E-mail: info@ligo.caltech.edu

Massachusetts Institute of Technology
LIGO Project - MS 20B-145
Cambridge, MA 01239
Phone (617) 253-4824
Fax (617) 253-7014
E-mail: info@ligo.mit.edu

WWW: http://www.ligo.caltech.edu/

1 ABSTRACT

This document summarizes the frequency response of the LIGO interferometer to length changes and to input beam noise. In particular, the robustness of the longitudinal error signals to small changes of the interferometer losses and the coupling of frequency noise into the gravitational wave band are derived in detail.

2 DEFINITIONS

An overview of the LIGO interferometer is shown in Fig. 1.

The arm cavity lengths can be expressed as common and differential arm lengths

$$L_C = \frac{L_1 + L_2}{2} \quad \text{and} \quad L_D = \frac{L_1 - L_2}{2} \tag{1}$$

Similarly, if l_1 and l_2 are the in-line and the off-line Michelson length, the recycling cavity length l_C and the Schnupp asymmetry l_D can be written as

$$l_C = \frac{l_1 + l_2}{2} \quad \text{and} \quad l_D = \frac{l_1 - l_2}{2} \tag{2}$$

We distinguish macroscopic and microscopic lengths, where we assume that the macroscopic lengths are chosen to exactly fulfill the resonance and the dark port conditions. The deviations

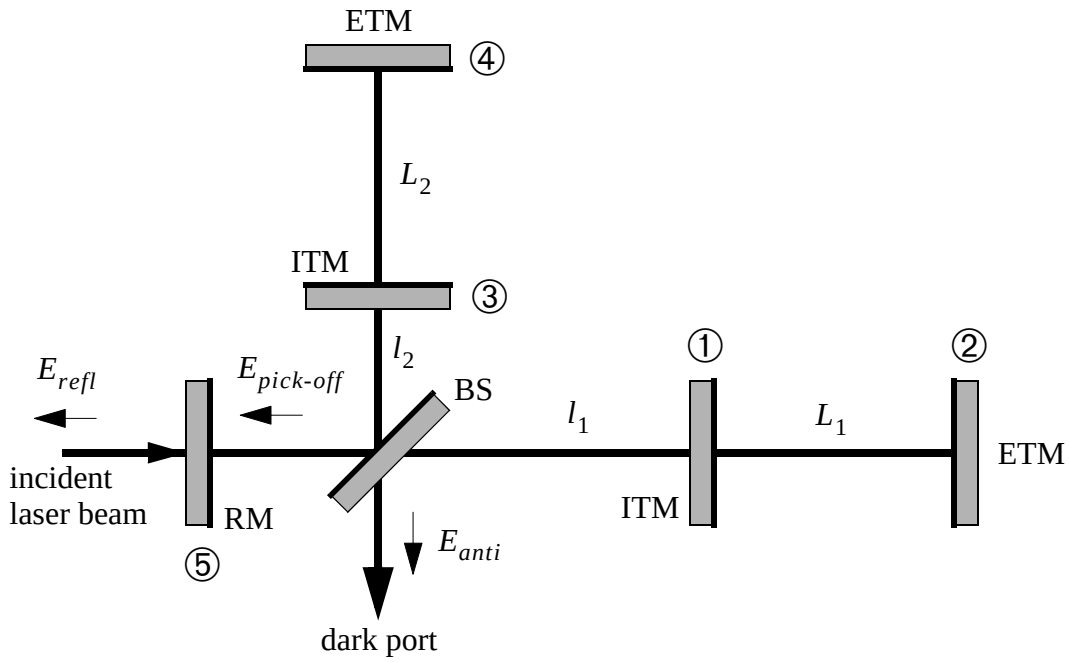

Figure 1: Configuration of the LIGO interferometer.

from resonance and the dark port conditions are subsequently denoted with a Δ prior to the corresponding length variable.

The recycling cavity of the LIGO interferometer can be related to a simple Fabry-Perot cavity by treating the Michelson and the two arm cavities as a compound mirror with reflectivity r_c for the carrier and reflectivity r_M for the rf sidebands, respectively. In case of the carrier the reflectivity is determined by the resonance reflectivity of the arm cavities, whereas for the rf sidebands the reflectivity is determined by the Michelson asymmetry.

$$r_c = \frac{r_1 - r_2}{1 - r_1 r_2} \quad \text{and} \quad r_M = \cos\frac{2\omega_m l_D}{c} \tag{3}$$

where r_1 and r_2 are the input and the rear mirror reflectivity of the arm cavities, ω_m is the modulation frequency and l_D is the asymmetry. The cavity reflectivity r_c is negative for an over-coupled cavity, positive for an under-coupled one and zero for a critically matched one. Since it will be used later on, we also give r_c' and $\hat{r}_c$ which describe the change in the reflected field of the arm cavity for carrier and rf sidebands, respectively, when the cavity length is changed (see also Appendix A):

$$r_c' = \frac{(1 - r_1^2) r_2}{(1 - r_1 r_2)^2} \quad \text{and} \quad \hat{r}_c = \frac{(1 - r_1^2) r_2}{(1 + r_1 r_2)^2} \tag{4}$$

where we assumed that the carrier is exactly resonant and that the rf sidebands are exactly anti-resonant.

One can now define amplitude gain, reflectivity and transmission coefficients as follows: g_{cr}^2 and g_{sb}^2 describe the recycling gain for carrier and rf sidebands, respectively, r_{cr} and r_{sb} describe the amplitude of the reflected field, t_{cr} and t_{sb} describe the field transmitted to the dark port.

$$\begin{aligned} g_{cr} &= \frac{t_5}{1 + r_5 r_c} & r_{cr} &= \frac{r_5 + r_c}{1 + r_5 r_c} & t_{cr} &= 0 \\ g_{sb} &= \frac{t_5}{1 - r_5 r_M} & r_{sb} &= \frac{r_5 - r_M}{1 - r_5 r_M} & t_{sb} &= \frac{t_5\sqrt{1 - r_M^2}}{1 - r_5 r_M} \end{aligned} \tag{5}$$

where r_5 and t_5 are the amplitude reflectivity and transmission of the recycling mirror. Since most of the measured signals are proportional to the input beam power and the modulation depth we usually give result in units of signal strength:

$$sig = 2 J_0(\Gamma) J_1(\Gamma) P_{in} \tag{6}$$

3 LONGITUDINAL TRANSFER FUNCTIONS

This section is a summary of the formulae given in M.W. Regehr's thesis.

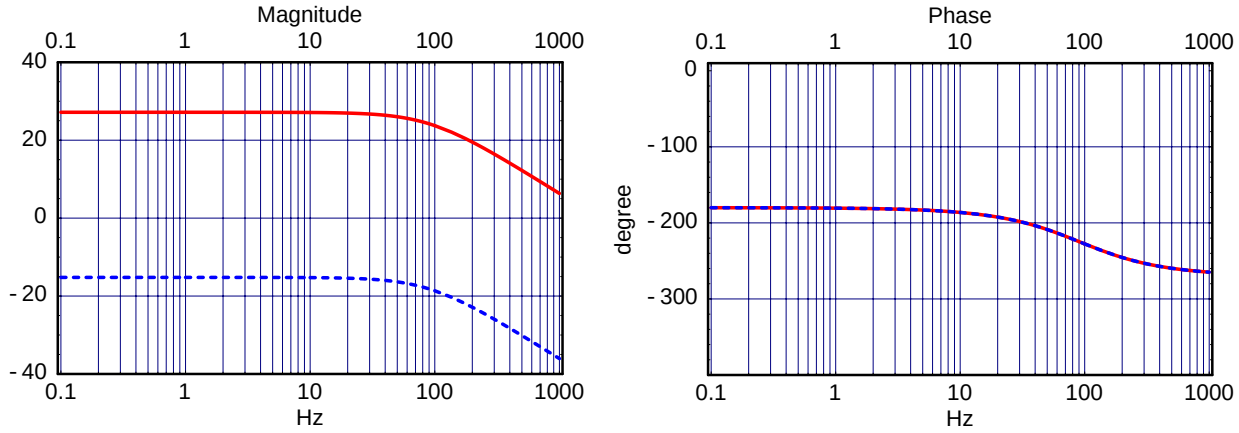

at the anti-symmetric port

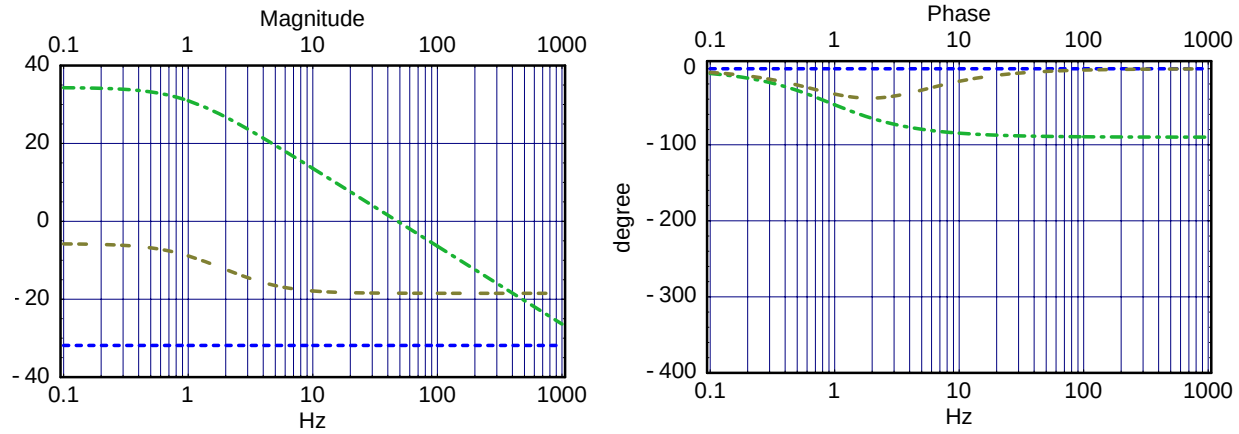

in reflection of the interferometer

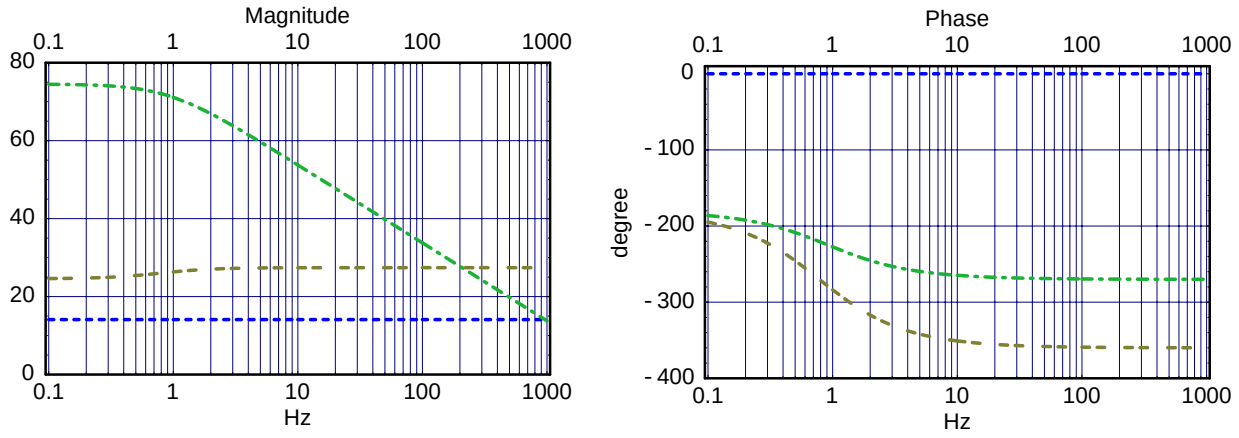

recycling cavity pick-off

Figure 2: Longitudinal transfer functions. Results are given for the differential (solid curve) and the common (dash-dotted) arm cavity length, the Michelson length (dashed) and the recycling cavity length (dash-dashed). The parameters used for the calculation are typical ones for LIGO with an over-coupled carrier and under-coupled rf sidebands. The magnitude of the signals are given in units of dB (sig/nm).

The following conventions are used:
i) only the rf signal at the modulation frequency is included in the result,
ii) the modulation is done with a cosine and, thus, cosine terms in the result are the 'in-phase' contribution, whereas sine terms are in the 'quad-phase',
iii) the results are normalized to the input power P_{in} and
iv) each result is given as a complex function of the audio sideband frequency, where its absolute value denotes the amplitude of the signal and its argument denotes the phase of the signal.

The signal at the anti-symmetric port is only sensitive to differential arm length and Michelson length changes.

$$\begin{aligned} S_{anti} \;=\; & -8J_0(\Gamma)J_1(\Gamma)P_{in}\, g_{cr} t_{sb} r_c' k\Delta L_D \frac{1}{1+s_c} \sin\omega_m t \\ & + 8J_0(\Gamma)J_1(\Gamma)P_{in}\, g_{cr} t_{sb} r_c\, k\Delta l_D \frac{1}{1+s_c} \sin\omega_m t \end{aligned} \tag{7}$$

Both signals from the differential arm length and the Michelson length do see the arm cavity pole. For the arm length change this is obvious, since the signal produced in the arm cavities falls out of the arm cavity resonance and, thus, its build-up is reduced. For the Michelson length the signal is produced inside the recycling cavity and the attenuation at higher frequencies happens because the carrier field experiences a sign change upon reflection of the arm cavity outside its resonance and, consequently, the signal falls out of resonance in the recycling cavity.

In reflection the in-phase signal is sensitive to changes in the common arm length and the recycling cavity length, whereas the quad-phase signal is mostly sensitive to the Michelson length.

$$\begin{aligned} S_{refl} \;=\; & -8J_0(\Gamma)J_1(\Gamma)P_{in}\, g_{sb} t_{sb} r_{cr} \hat{r}_c k\Delta L_D \sin\omega_m t \\ & -8J_0(\Gamma)J_1(\Gamma)P_{in}\, g_{sb} t_{sb} r_{cr} k\Delta l_D \sin\omega_m t \\ & +8J_0(\Gamma)J_1(\Gamma)P_{in}\, g_{cr}^2 r_{sb} r_c' k\Delta L_C \frac{1}{1+s_{cc}} \cos\omega_m t \\ & -8J_0(\Gamma)J_1(\Gamma)P_{in}\, [g_{cr}^2 r_{sb} r_c + g_{sb}^2 r_{cr} r_M] k\Delta l_C \frac{1+s_r}{1+s_{cc}} \cos\omega_m t \end{aligned} \tag{8}$$

where the zero in the transfer function of the recycling cavity length is at

$$s_r \;=\; \frac{i\omega_a}{\omega_r} \quad \text{with} \quad \omega_r \;=\; \left(1 + \frac{g_{cr}^2 r_{sb} r_c}{g_{sb}^2 r_{cr} r_M}\right)\omega_{cc} \tag{9}$$

Since the signals in the quad-phase are produced by a change in the rf sidebands which is then measured by their beating against the static carrier field, there is no frequency dependence of these signals below the recycling cavity pole and their signs depend only on the coupling of the carrier field into the interferometer. In particular, if the carrier is critically matched the quad phase signals become identical zero. Since the in-phase signals originating from a common arm length

change is caused by a change of the carrier field alone it sees nothing else but the double cavity pole. The situation is more complicated for the in-phase signal originating from a recycling cavity length. Here, both the carrier and the rf sidebands participate to the signal, however, with an important difference: the carrier sees the double resonance, whereas the rf sidebands don't. Adding the two signals together gives a transfer function consisting of the double cavity pole and an additional zero at a frequency ω_r. As can be seen from eqn. (9) this zero can lie on either side of the s-plane. In case of a right half plane zero, it will cause the signal amplitude to rise by simultaneously introducing a phase lag. It should also be noted that the signs of the in-phase signals do not depend on the coupling of the carrier into the interferometer, but rather on the ratio of the recycling gain of carrier and rf sidebands.

At the pick-off of the recycling cavity the situation is very similar to the one in reflection.

$$\begin{aligned} S_{pick\text{-}off} \;=\; & +8J_0(\Gamma)J_1(\Gamma)P_{in}\frac{g_{cr}g_{sb}}{t_5}t_{sb}\hat{r}_c\,k\Delta L_D\sin\omega_m t \\ & +8J_0(\Gamma)J_1(\Gamma)P_{in}\frac{g_{cr}g_{sb}}{t_5}t_{sb}\,k\Delta l_D\sin\omega_m t \\ & -8J_0(\Gamma)J_1(\Gamma)P_{in}\frac{g_{cr}^2 g_{sb}}{t_5}r_M r_c'k\Delta L_C\frac{1}{1+s_{cc}}\cos\omega_m t \\ & +8J_0(\Gamma)J_1(\Gamma)P_{in}\frac{g_{cr}g_{sb}}{t_5}r_M r_c[g_{cr}-g_{sb}]k\Delta l_C\frac{1+s_p}{1+s_{cc}}\cos\omega_m t \end{aligned} \tag{10}$$

where the zero in the transfer function of the recycling cavity length is at

$$s_p \;=\; \frac{i\omega_a}{\omega_p} \quad \text{with} \quad \omega_p \;=\; \left(1-\frac{g_{cr}}{g_{sb}}\right)\omega_{cc} \tag{11}$$

There are some important differences, however. The quad-phase signal from the Michelson length change does not depend on the coupling of the carrier into the interferometer anymore and it is non-zero even when the carrier is critically coupled. The sign of the signal from the recycling cavity length only depends on the relative size of the recycling gain of carrier and rf sidebands. The same is true for the location of the zero: if the carrier recycling gain is larger than the one of the rf sidebands, the zero lies in the right half plane.

Since both the in-phase signal in reflection and at the pick-off are so much more sensitive to the common arm cavity length than they are to the recycling cavity length, a real world servo application would generally use one of the signals to feed back to laser wavelength with a fairly high bandwidth. This in turn will make the other signal mostly sensitive to the recycling cavity length. For example, enforcing $S_{refl}(\text{in-phase}) = 0$ by adjusting ΔL_C will lead to a remaining signal $S'_{pick\text{-}off}$ at the recycling cavity pick-off which is entirely due to the recycling cavity length deviation from resonance:

$$S'_{pick\text{-off}}(\text{in-phase}) \;=\; -8J_0(\Gamma)J_1(\Gamma)P_{in}\frac{g_{sb}^2 r_M}{t_5 r_{sb}}[g_{cr}r_{sb}r_c + g_{sb}r_{cr}r_M]k\Delta l_C\cos\omega_m t \tag{12}$$

Surprisingly, this signal is now completely frequency independent! Expanding the sum term of eqn. (12) with the help of eqns. (5) one finds

$$g_{cr} r_{sb} r_c + g_{sb} r_{cr} r_M \propto r_M + r_c \tag{13}$$

and the sign of the signal only depends on the relative size of the recycling gain of carrier and rf sidebands and on the sign of the reflected rf sideband field. Analogously, one can look at the signal in reflection when the pick-off signal is driven to zero by adjusting the common arm cavity length

$$S'_{refl}(\text{in-phase}) \;=\; -8 J_0(\Gamma) J_1(\Gamma) P_{in}\, g_{sb} [g_{cr} r_{sb} r_c + g_{sb} r_{cr} r_M] k \Delta l_C \cos\omega_m t \tag{14}$$

4 Noise on the Input Laser Beam

This derivation was taken from LIGO-T960019-00-D. The used audio sideband equations are given in Appendix A and the formulae for the down-conversion are given in Appendix B. In brief, we treat noise on the input laser light as additional components at frequencies separated from the carrier and the rf sidebands by an audio sideband frequency ω_a. A summary of the added frequency components on the input laser light due to laser frequency noise, laser amplitude noise, oscillator frequency noise and oscillator amplitude noise are listed in Table 1. We then calculated the response of the interferometer to these additional frequencies at the dark port, in reflection and at the pick-off of the recycling cavity. Especially important are the quad-phase contributions at the dark port, because they compete with the gravitational wave signal. Most of these noise sources couple through interferometer imperfections to the dark port, especially in the presence of unwanted (static) carrier light. Fundamentally, there are two types of carrier leakages: (1) the differential arm length is slightly off-resonance and carrier field amplitude at the dark port becomes purely imaginary and (2) the reflectivities of the two Michelson arms are different and the carrier field amplitude at the dark port becomes purely real. The first effect is conveniently parametrized by the differential arm length deviation ΔL_D, whereas the second effect is accounted for by introducing an arm cavity reflectivity difference δr_c and by adding an arbitrary field amplitude $g_{cr} C$ to the static carrier light at the dark port.

4.1 RF Modulation

Neglecting the effects of noise for a moment the rf phase modulation on the input laser beam can be written as

$$E_{in} \;=\; e^{i\Gamma\cos\omega_m t} E_0 \approx \left\{ J_0(\Gamma) + i J_1(\Gamma) e^{-i\omega_m t} + i J_1(\Gamma) e^{+i\omega_m t} \right\} E_0 \tag{15}$$

where E_0 is a pure TEM_{00} mode coming out of the laser, Γ is the modulation depth and ω_m is the modulation frequency.

Table 1: Summary of the noise on the input laser light.

Modulation	$-\omega_m$			0			$+\omega_m$		
Audio sideband	$-\omega_a$	0	$+\omega_a$	$-\omega_a$	0	$+\omega_a$	$-\omega_a$	0	$+\omega_a$
Frequency noise	$-iJ_1\frac{f_N}{2}$	iJ_1	$iJ_1\frac{f_N}{2}$	$-\frac{f_N}{2}$	J_0	$\frac{f_N}{2}$	$-iJ_1\frac{f_N}{2}$	iJ_1	$iJ_1\frac{f_N}{2}$
Amplitude noise	$iJ_1\frac{\Delta A}{2A}$	iJ_1	$iJ_1\frac{\Delta A}{2A}$	$\frac{\Delta A}{2A}$	J_0	$\frac{\Delta A}{2A}$	$iJ_1\frac{\Delta A}{2A}$	iJ_1	$iJ_1\frac{\Delta A}{2A}$
Oscillator phase noise	$iJ_1\frac{\Delta\Gamma}{2\Gamma}$	iJ_1	$iJ_1\frac{\Delta\Gamma}{2\Gamma}$	0	J_0	0	$iJ_1\frac{\Delta\Gamma}{2\Gamma}$	iJ_1	$iJ_1\frac{\Delta\Gamma}{2\Gamma}$
Oscillator amplitude noise	$J_1\frac{\phi_o}{2}$	iJ_1	$J_1\frac{\phi_o}{2}$	0	J_0	0	$-J_1\frac{\phi_o}{2}$	iJ_1	$-J_1\frac{\phi_o}{2}$

4.2 FREQUENCY NOISE

Frequency noise is described by adding a noise term to the laser frequency

$$f(\omega_a) = f + \delta f \cos\omega_a t \tag{16}$$

The corresponding phase is then

$$\varphi(t) = 2\pi\int_0^t f(\omega_a)\,dt = 2\pi f t + f_N \sin\omega_a t \quad \text{with} \quad f_N = \frac{2\pi\delta f}{\omega_a} \tag{17}$$

The last term of eqn. (17) produces an additional phase modulation on the input light

$$E'_{in} = e^{if_N\sin\omega_a t}E_{in} \approx \left\{1 + \frac{f_N}{2}[e^{+i\omega_a t} - e^{-i\omega_a t}]\right\}E_{in} \tag{18}$$

Using eqns. (49) and (55) for the interferometer operator and the first line of Table 1 as the noise operator we obtain the rf signal at the anti-symmetric port due to frequency noise.

$$S_{anti}^{f_N} = -2J_0(\Gamma)J_1(\Gamma)P_{in}\,g_{cr}\,t_{sb}\,f_N\left\{\sin\omega_m t\right. \tag{19}$$

$$\left[4i\frac{\omega_c l_D}{c}r_c\frac{(1+s_c/r_c)s_c}{1+s_{cc}} + i\frac{\delta\omega_c}{\omega_c}\frac{(1-r_c)s_c}{(1+s_{cc})(1+s_c)} + i(\delta r_c + 2C)\frac{s_{cc}}{1+s_{cc}}\right] +$$

$$\left. ir_{sb}s_m[\delta r_c + 2C]\cos\omega_m t\right\}$$

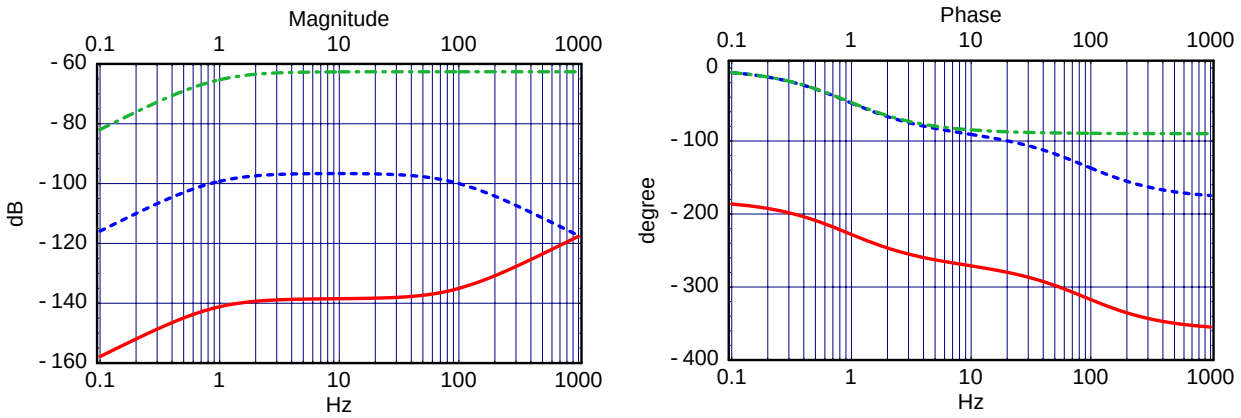

Figure 3: Phase (frequency) noise coupling. Plotted is the phase noise at the dark port for caused by the Schnupp asymmetry (solid curve), by a difference of the arm cavity pole frequency of 100 ppm (dashed) and by difference in the arm cavity reflectivity of 100 ppm. The magnitude of the signals are given in units of dB (sig/rad). (We do not imply that 100 ppm are realistic imperfections.)

The coupling of phase noise of the input beam into the gw-signal at the anti-symmetric port is shown in Fig. 3. All of the signals show the double cavity pole which acts as a high pass filter. In case of the Schnupp asymmetry the signal is produced by a the carrier audio sidebands which leak out at the dark port. This signal is filtered by the double cavity resonance up to the arm cavity pole above which the audio sidebands are prompt reflected by the arms. The difference of the arm cavity poles will cause a difference in phase shift for the carrier audio sidebands entering the arm cavities. Since the coupling of the carrier audio sidebands into the arm cavities vanishes above the arm cavity pole, this effects is decreasing at high frequencies. The third effect has a different origin: the difference in reflectivities between the arm cavities causes carrier light to leak out at the dark port as a contrast defect. Normally, this wouldn't pose a problem, because the audio sidebands of carrier and rf sidebands would cancel each other. However, above the double cavity pole the audio sidebands of the carrier are stripped off, leaving the audio sidebands of the rf sidebands now beating against the static carrier (TEM_{00}) contrast defect. Note, that the differential arm length error signal is in the 'wrong phase' and will not contribute to this effect.

Since the signals in reflection and at the pick-off of the recycling cavity are first order sensitive to frequency noise we will neglect the small terms coming from interferometer imperfections.

$$S^{f_N}_{pick\text{-}off} = 4J_0(\Gamma)J_1(\Gamma)P_{in}\, g_{cr} g_{sb}\, r_M\, f_N \frac{1-r_c}{1+r_5}\frac{is_{cc}}{1+s_{cc}}\cos\omega_m t \quad \text{and} \tag{20}$$

$$S^{f_N}_{refl} = -4J_0(\Gamma)J_1(\Gamma)P_{in}\, r_{sb}\, f_N (1-r_{cr})\frac{is_{cc}}{1+s_{cc}}\cos\omega_m t \tag{21}$$

Since it is unlikely that the intrinsic frequency noise on the input light of the interferometer is small enough to be negligible compared to the required gravitational wave sensitivity at the dark

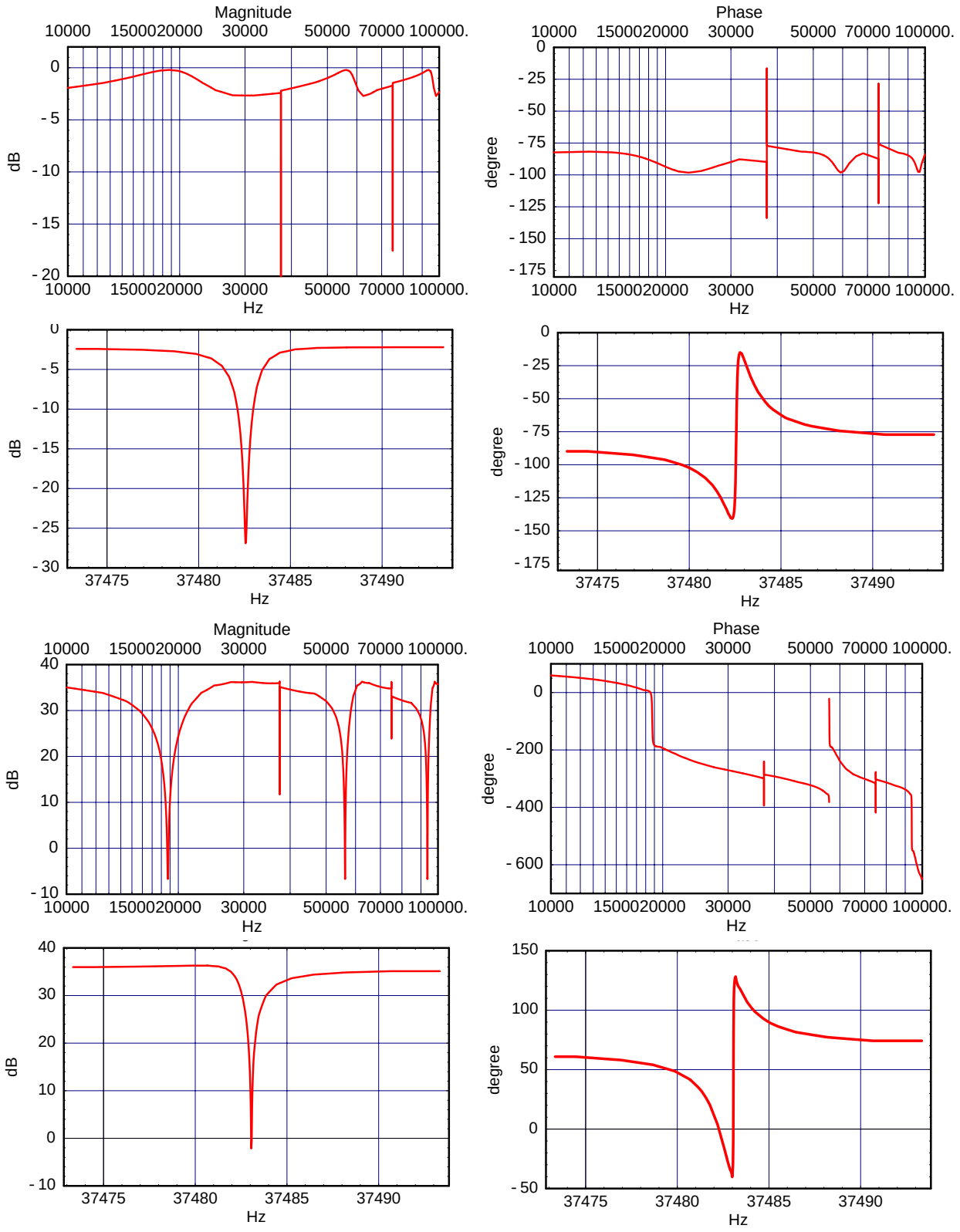

Figure 4: Phase (frequency) noise coupling in reflection (upper half) and at the recycling cavity pick-off. The magnitude of the signals are given in units of dB (sig/rad).

port, one would generally take either the reflected or the pick-off signal and feed it back to the laser wavelength.

Fig. 4 shows the frequency noise coupling into the signal in reflection and at the recycling cavity pick-off for frequencies above 10 kHz where eqns. (20) and (21) are not good approximations anymore. The first feature shows up at half the free-spectral-range where the rf-sidebands are becoming resonance in the arm cavities. Since this means that they are falling out of resonance in the recycling cavity and are now prompt reflected at the recycling mirror, the signal at the pick-off goes through zero and changes sign, whereas the signal in reflection shows a hump. The next feature shows up at the free-spectral-range when the carrier hits the double-resonance again. Because the rf-sidebands are now slightly detuned in the recycling cavity, the signals in reflection and at the pick-off don't vanish exactly — like one would expect if the transfer functions would repeat themselves every free-spectral-range.

4.3 AMPLITUDE NOISE

The amplitude noise in the input beam at audio frequencies is described by

$$E'_{in} = \left(1 + \frac{\Delta A}{A}\right)\cos\omega_a t \; E_{in} \tag{22}$$

Both amplitude noise at audio and at rf frequencies can effect the dark port signal. Using eqns. (49) and (55) for the interferometer operator and the second line of Table 1 as the input beam noise one obtains an rf signal at the dark port due to low frequency amplitude noise.

$$S^A_{anti} = -8J_0(\Gamma)J_1(\Gamma)P_{in}\, g_{cr} t_{sb} r_c' \frac{\Delta A}{A} k\,\Delta L_D \tag{23}$$

$$\left\{\left[1 + \frac{1}{(1+s_{cc})(1+s_c)}\right]\sin\omega_m t + r_{sb} s_m \cos\omega_m t\right\}$$

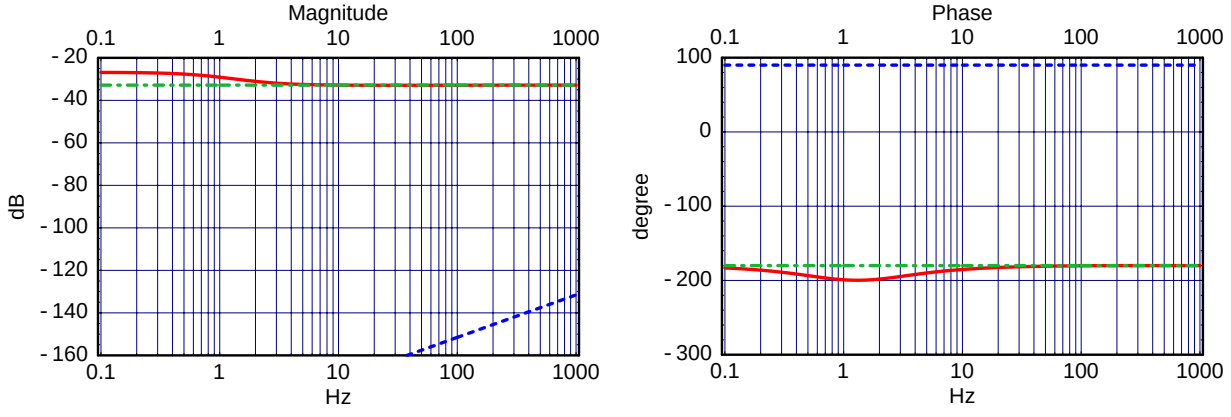

Figure 5: Laser amplitude noise (solid curve), oscillator phase noise (dashed) and oscillator amplitude noise coupling to the gw-signal. The magnitude of the signals at the dark port are given in units of dB (sig/modulation depth or sig/rad) assuming $\Delta L_D = 10^{-12}$.

The low frequency laser amplitude noise couples through a differential arm cavity length offset to the anti-symmetric port. Audio sidebands from both the carrier and the rf sidebands contribute to the signal. Above the double cavity pole the audio sidebands of the carrier are filtered out, effectively cutting the signal in half.

For the signal at the pick-off of the recycling cavity and in reflection of the interferometer one obtains:

$$S^{A}_{pick\text{-}off} = 4J_0(\Gamma)J_1(\Gamma)P_{in}\, g_{cr} g_{sb} r_M r_c' \frac{\Delta A}{A}\, k\, \Delta L_C \frac{2 + s_{cc}}{1 + s_{cc}} \cos\omega_m t \quad \text{and} \tag{24}$$

$$S^{A}_{refl} = -4J_0(\Gamma)J_1(\Gamma)P_{in}\, g_{cr}\sqrt{1 - r_5^2}\, r_{sb} r_c' \frac{\Delta A}{A} k \Delta L_C \left[1 + \frac{1}{(1 + s_{cc})(1 + s_c)}\right] \cos\omega_m t \tag{25}$$

We now investigate the effect of amplitude noise at the rf frequency by modulate the incident laser beam in amplitude — instead of phase —

$$E_{in} = \left(1 + \frac{\Delta A'}{A'}\cos\omega_m t\right) E_0 = \left\{1 + \frac{\Delta A'}{2A'} e^{-i\omega_m t} + \frac{\Delta A'}{2A'} e^{+i\omega_m t}\right\} E_0 \tag{26}$$

and calculate the signal at the dark port:

$$S^{A'}_{anti} = -P_{in}\, g_{cr}\, t_{sb} \frac{\Delta A'}{A'} \{2C + \delta r_c\} \sin\omega_m t \tag{27}$$

4.4 Oscillator Phase Noise

Oscillator phase noise in the input beam is obtained by adding a frequency noise term to the rf phase modulator

$$E'_{in} = e^{i\Gamma\cos(\omega_m t + \phi_o \cos\omega_a t)} E_0 \approx \left\{ J_o(\Gamma) + iJ_1(\Gamma)\left[e^{+i\omega_m t} + e^{-i\omega_m t} + \frac{i\phi_o}{2}\left(e^{i(\omega_m + \omega_a)t} + e^{i(\omega_m - \omega_a)t} - e^{-i(\omega_m + \omega_a)t} - e^{-i(\omega_m - \omega_a)t}\right)\right]\right\} E_0 \tag{28}$$

Oscillator phase noise not only adds noise to the input beam, but also adds noise to the local oscillator signal used for the down-conversion. The latter effects is negligible for the quad-phase signal, since only small noise terms exist in the in-phase of the dark port signal which would be mixed into the gw-signal by the oscillator phase noise. For the in-phase signal the situation is very different: its audio signal is produced by a static carrier field leaking out the dark port. This carrier field also produces a static signal in the quad phase which in turn is mixed into the in-phase by the oscillator phase noise and which cancels the other signal in the in-phase.

$$S^{\phi_o}_{anti} = 8J_0(\Gamma)J_1(\Gamma)P_{in}\, g_{cr}\, t_{sb}\, r_c' \phi_o\, k\, \Delta L_D r_{sb}\, s_m \sin\omega_m t \tag{29}$$

We conclude that oscillator phase noise only couples through the (audio) frequency dependency of the rf sideband amplitudes in the recycling cavity and through a differential arm cavity length deviation into the gw-signal. Because the signal in reflection and at the recycling cavity pick-off are in the in-phase, there is no first order coupling of oscillator phase noise to them.

4.5 Oscillator Amplitude Noise

Oscillator amplitude noise in the input beam is obtained by adding an amplitude modulation to the modulation depth Γ:

$$E'_{in} = e^{i\Gamma\left(1+\frac{\Delta\Gamma}{\Gamma}\cos\omega_a t\right)\cos\omega_m t} E_0 \approx \tag{30}$$

$$\left\{J_o(\Gamma) + iJ_1(\Gamma)\left[1+\frac{i\phi_o}{2}(e^{i\omega_a t}+e^{i\omega_a t})\right][e^{+i\omega_m t}+e^{-i\omega_m t}]\right\}E_0$$

The coupling of oscillator amplitude noise into the gw-signal is very similar to the one of the oscillator phase noise, but with quad- and in-phase interchanged. There is also no contribution from the down-conversion due to the limiter amplifier implemented into the rf mixer. The signal at the dark port reads

$$S_{anti}^{\Delta\Gamma} = -8J_0(\Gamma)J_1(\Gamma)P_{in}g_{cr}t_{sb}r_c'\frac{\Delta\Gamma}{\Gamma}k\Delta L_D\{\sin\omega_m t + r_{sb}s_m\cos\omega_m t\} \tag{31}$$

which is identical to the laser amplitude noise above the double cavity pole. The same holds true for the signal in reflection and at the pick-off of the recycling cavity which are identical to the laser amplitude noise coupling above the double cavity pole.

4.6 Shot Noise

When considering the effect of input beam noise on the measured signals, one important comparison is the shot noise. Of course, any signal from the input beam noise which lies significantly below shot noise is irrelevant. On the anti-symmetric port and in reflection it is principle possible to detect all the light, whereas at the recycling cavity pick-off only a small fraction of the circulating light $f_{pick\text{-}off}$ can actually be detected without significantly reducing the recycling gain. Neglecting the quantum efficiency of the photodetector and using $h\nu$ for the photon energy and c_d for the contrast defect at the anti-symmetric port the shot noise is:

$$S_{anti}^{SN} = 2\sqrt{\left[J_0(\Gamma)^2 g_{cr}^2\frac{c_d}{2} + 3J_1(\Gamma)^2 t_{sb}^2\right]P_{in}\,h\nu}$$

$$S_{refl}^{SN} = 2\sqrt{[J_0(\Gamma)^2 r_{cr}^2 + 3J_1(\Gamma)^2 r_{sb}^2]P_{in}\,h\nu} \tag{32}$$

$$S_{pick\text{-}off}^{SN} = 2\sqrt{[J_0(\Gamma)^2 g_{cr}^2 + 3J_1(\Gamma)^2 g_{sb}^2]\,f_{pick\text{-}off}P_{in}\,h\nu}$$

where we included a factor of $\frac{3}{2}$ for the non-stationary noise of the rf sidebands and an overall factor of $\sqrt{2}$ which accounts for the frequency folding in the down-conversion.

5 RESULTS

5.1 ERROR SIGNAL ROBUSTNESS

To characterize the robustness of the longitudinal error signals to small changes in the interferometer configuration their signs are listed in Table 2 for a different carrier and rf sideband couplings. If both carrier and rf sidebands have the same coupling to the interferometer we also distinguish which one has the higher recycling gain. If the sign of an error signal changes when, say, the carrier changes from over- to undercoupled it actually vanishes in case the carrier is exactly critically matched. Similarly, if carrier and rf sidebands have identical recycling gain, the signal due to the recycling cavity length vanishes. In practice, the most relevant case is when carrier is coming close to critically matched. On the one hand one would like to start with an undercoupled carrier which would then become even more undercoupled if the interferometer acquires additional losses. On the other hand, the carrier coupling is only determined by the reflectivity of the recycling mirror and the losses in the interferometer and, if one underestimates the initial quality of the optics one might end up with an overcoupled system rather than an undercoupled one. Therefore, it is an advantage if none of the error signals vitally depends on the carrier coupling. Indeed, this can be achieved by measuring the Michelson length at the recycling cavity pick-off, rather than in reflection. Since the coupling of the rf sidebands can be selected either way by the length of the asymmetry, it can always be optimized for a given set of optics afterwards.

Table 2: Signs of error signals.

coupling		build-up	L_D	l_D		L_C		l_C	
carrier	**sidebands**	**RC**	**dark**	**refl.**	**RC**	**refl.**	**RC**	**RC[1]**	**refl.[2]**
over	over	$g_{cr} < g_{sb}$	–	+	+	–	–	+	–
over	over	$g_{cr} > g_{sb}$	–	+	+	–	–	–	+
over	under	$g_{cr} > g_{sb}$	–	+	+	+	–	+	+
under	under	$g_{cr} > g_{sb}$	–	–	+	+	–	+	+
under	under	$g_{cr} < g_{sb}$	–	–	+	+	–	–	–
under	over	$g_{cr} < g_{sb}$	–	–	+	–	–	+	–

1. Assumes that the signal in reflection is driven to zero by adjusting L_C.
2. Assumes that the signal at the recycling cavity (RC) pick-off is driven to zero by adjusting L_C.

5.2 Frequency Noise Suppression

Since the frequency noise suppression one can achieve prior to the interferometer is not sufficient to guarantee the required gravitational wave sensitivity, one has to use the interferometer itself as a reference cavity and feed the common arm cavity error signal back to the frequency stabilization. One of the limiting factors in this scheme is the shot noise seen by the detector in reflection or at the recycling cavity pick-off. Fig. 6 compares the shot noise induced frequency noise as seen at the dark port to the shot noise limited gravitational wave sensitivity. Only the signal in reflection has a signal-to-noise ratio large enough to provide the error signal for the frequency stabilization. For the calculation it was assumed that all the light in reflection is available, that 300 ppm of the light inside the recycling cavity is extracted at the pick-off and that the difference in amplitude reflectivity of the two arm cavities is 0.46% which corresponds to a 70 ppm difference in round-trip losses.

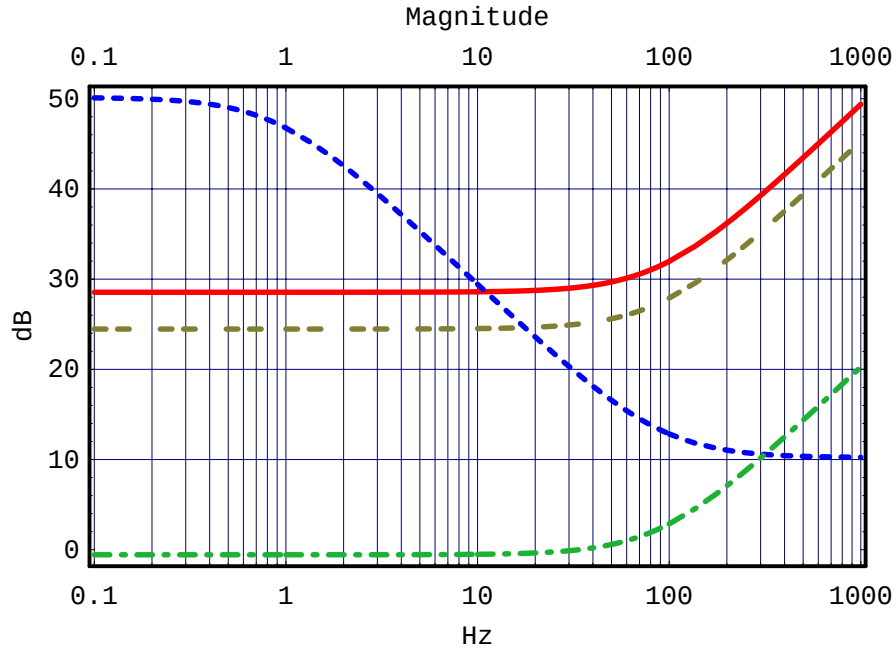

Figure 6: Frequency noise suppression. Shown is the shot noise limited gravitational wave sensitivity (solid curve) and the shot noise induced frequency noise for the signal in reflection (dash-dotted) and for the signal at the recycling cavity pick-off (dash-dashed). As a comparison the dashed curve shows a constant frequency noise level of $10^{-7}\,\mathrm{Hz}/\sqrt{\mathrm{Hz}}$. The units are dB of 10^{-21} m of differential arm length change. The difference in round-trip losses between the two arm cavities was assumed to be 70 ppm.

APPENDIX A AUDIO SIDEBAND EQUATIONS

A.1 ARM CAVITY

If we write the input field as $E_{in} = e^{i(\omega + \omega_a)t}$, the field inside the arm cavity is given by

$$E_{arm} = \frac{\sqrt{1-r_1^2}}{1 - r_1 r_2 e^{-2i\omega_a l/c}} E_{in} \tag{33}$$

where r_1 and r_2 are the amplitude reflectivity coefficients of the input and the rear mirror respectively, ω_a is the (audio) frequency deviation from resonance, l is the cavity length and ϕ is the phase deviation from resonance. For the light in reflection and in transmission one obtains

$$E_{refl}^{arm} = r_1 E_{in} - r_2 \sqrt{1-r_1^2} e^{-2i\omega_a l/c} E_{arm} \tag{34}$$

$$E_{trans}^{arm} = \sqrt{1-r_2^2} e^{-i\omega_a l/c} E_{arm} \tag{35}$$

Using the 'cavity pole' notation

$$s_c \equiv \frac{i\omega_a}{\omega_c} \quad \text{and} \quad \omega_c = \frac{c}{2l} \frac{1 - r_1 r_2}{\sqrt{r_1 r_2}} \tag{36}$$

and making the assumption that

$$\frac{\omega_a}{2\pi} \ll \frac{c}{2l} \tag{37}$$

one can write eqns. (33), (34) and (35) as

$$E_{arm} = \left(\frac{\sqrt{1-r_1^2}}{1 - r_1 r_2} \frac{1}{1 + s_c} - 2i\,k\,\Delta l \frac{r_1 r_2 \sqrt{1-r_1^2}}{(1 - r_1 r_2)^2} \frac{1}{(1 + s_c)^2} \right) E_{in} \tag{38}$$

$$E_{refl}^{arm} = \left(r_c \frac{1 + s_c / r_c}{1 + s_c} + 2i \frac{r_c' \, k \, \Delta l}{(1 + s_c)^2} \right) E_{in} \tag{39}$$

$$E_{trans}^{arm} = \frac{\sqrt{1-r_1^2}\sqrt{1-r_2^2}}{1 - r_1 r_2} \left(\frac{1}{1 + s_c} - i\,k\,\Delta l \frac{1 + r_1 r_2}{1 - r_1 r_2} \frac{1}{(1 + s_c)^2} \right) E_{in} \tag{40}$$

where r_c is the resonance reflectivity of the arm cavity and r_c' is the its derivative in respect to the arm cavity round trip phase — see also eqns. (3) and (4):

$$\frac{c}{2l}\frac{dE_{refl}^{arm}}{d\omega_a}\bigg|_{\omega_a = 0} \equiv i r_c' E_{in} \tag{41}$$

For the rf sidebands the derivative becomes

$$\frac{c}{2l}\frac{d}{d\omega_a}E_{refl}^{arm}(\omega_m + \omega_a)\bigg|_{\omega_a = 0} \equiv i\hat{r}_c\, E_{in} \quad \text{with} \quad \hat{r}_c(\omega_m) = \frac{(1-r_1^2)r_2 e^{-i\omega_m/FSR}}{(1-r_1 r_2 e^{-i\omega_m/FSR})^2} \tag{42}$$

where $FSR = c/2l$ is the free spectral range of the arm cavity. In case the rf sidebands are anti-resonant one obtains the result from eqn. (4):

$$\hat{r}_c(\omega_m \to 2\pi(n+\tfrac{1}{2})FSR) \to \hat{r}_c \tag{43}$$

A.2 Power Recycling Cavity

The equation for the field E_{RC} just after the recycling mirror is

$$E_{RC} = \frac{\sqrt{1-r_5^2}}{1 + \frac{r_5}{2}e^{-2i(\omega_m+\omega_a)l_C/c}\left\{G_1 e^{-2i(\omega_m+\omega_a)l_D/c} + G_2 e^{+2i(\omega_m+\omega_a)l_D/c}\right\}} E_{in} \tag{44}$$

where G_1 and G_2 are the arm cavity operators, l_C and l_D are the recycling cavity and the Michelson differential lengths, respectively, and r_5 is the amplitude reflectivity of the recycling mirror. The fields E_{anti} at the dark port, E_{refl} in reflection of the interferometer and $E_{pick\text{-}off}$ at the pick-off of the recycling cavity then become

$$E_{anti} = \frac{1}{2}\left\{G_1 e^{-2i(\omega_m+\omega_a)l_D/c} - G_2 e^{+2i(\omega_m+\omega_a)l_D/c}\right\}E_{RC} \tag{45}$$

$$E_{pick\text{-}off} = \frac{1}{2}\left\{G_1 e^{-2i(\omega_m+\omega_a)l_D/c} + G_2 e^{+2i(\omega_m+\omega_a)l_D/c}\right\}E_{RC} \tag{46}$$

$$\text{and} \quad E_{refl} = r_5 E_{in} + \sqrt{1-r_5^2}E_{pick\text{-}off} \tag{47}$$

A.2.1 RF Sidebands

Since the rf sidebands are not resonant in the arm cavities, $G_1 = G_2 = -1$, their frequency response is ‘flat’ up to the cavity pole of the recycling cavity. Note that the minus sign in G comes from the fact that recycling cavity was made resonant for the carrier assuming overcoupled

arm cavities, thus, the sidebands also have to pick up a minus sign, but in the round-trip phase. Making the approximation that the audio sideband frequency is much smaller than the free-spectral range of the arm cavities

$$\omega_a \ll \frac{c}{2l_C}\frac{1-r_5}{\sqrt{r_5}} \tag{48}$$

one obtains for the fields at the extraction ports:

$$E_{anti} = it_{sb}(\omega_m)\{1 + ir_{sb}(\omega_m)\, s_m\}E_{in} \quad \text{with } s_m = i\frac{\omega_a}{\omega_m}, \tag{49}$$

$$E_{pick\text{-}off} = -g_{sb}r_M E_{in} \quad \text{and} \quad E_{refl} = r_{sb}E_{in} \tag{50}$$

A.2.2 CARRIER FIELD

Using eqn. (39) the arm cavity operator G is defined as

$$G(\omega_a, \omega_c, r_c) = r_c\frac{1 + s_c/r_c}{1 + s_c} \quad \text{with } s_c = i\frac{\omega_a}{\omega_c} \tag{51}$$

Setting $G_1 = G_2 = G(\omega_a, \omega_c, r_c)$ the resonant carrier field can be written as

$$E_{RC} = g_{cr}\frac{1 + s_c}{1 + s_{cc}}E_{in} \quad \text{with } s_{cc} = i\frac{\omega_a}{\omega_{cc}} \text{ and } \omega_{cc} = \frac{1 + r_5 r_c}{1 + r_5}\omega_c \tag{52}$$

where ω_{cc} denotes the double cavity pole. To derive E_{RC} we neglected effects coming from differences in arm cavity storage times and in arm cavity reflectivities. Because these are differential effects the symmetric path of the recycled Michelson is not sensitive to them in first order. For the fields at the pick-off and in reflection one obtains

$$E_{pick\text{-}off} = g_{cr}r_c\frac{1 + s_c/r_c}{1 + s_{cc}}E_{in} \quad \text{and} \quad E_{refl} = r_{cr}\frac{1 + s_{cc}/r_{cr}}{1 + s_{cc}}E_{in} \tag{53}$$

To obtain the field at the dark port we set

$$G_1 = G\left(\omega_a, \omega_c + \frac{\delta\omega_c}{2}, r_c + \frac{\delta r_c}{2}\right) \quad \text{and} \quad G_2 = G\left(\omega_a, \omega_c - \frac{\delta\omega_c}{2}, r_c - \frac{\delta r_c}{2}\right) \tag{54}$$

and after a few ‘simple’ algebraic manipulations

$$E_{anti} = \frac{1}{2}\left\{-4r_c\frac{\omega_c l_D}{c}\frac{(1 + s_c/r_c)s_c}{1 + s_c} - \frac{\delta\omega_c}{\omega_c}\frac{(1 - r_c)s_c}{(1 + s_c)^2} + \frac{\delta r_c}{r_c}\frac{r_c}{1 + s_c} + 4i\frac{r_c' k\Delta L_D}{(1 + s_c)^2} + C\right\}E_{RC} \tag{55}$$

where we added the constant C to account for a contrast defect in the real phase. The dark port signal due to this contrast defect is then identical zero, since it is in the ‘wrong phase’.

APPENDIX B DOWN CONVERSION

If we now use the operators $O(\omega_m, \omega_a)$ and $N(\omega_m, \omega_a)$ to denote the frequency response of the interferometer and the noise added to the input beam, the field at the output port can be written as

$$E_{out} = \sum_{\omega_m, \omega_a} O(\omega_m, \omega_a) N(\omega_m, \omega_a) E_0(\omega_m, \omega_a) \tag{56}$$

where the input field is given by

$$E_0(\omega_m, \omega_a) = \sqrt{\frac{P_{in}}{2}} e^{i(\omega + \omega_m + \omega_a)t} \tag{57}$$

We obtain the rf signal which is relevant for the down conversion by looking at the power at the output port and including only terms proportional to $\cos\omega_m t$ and $\sin\omega_m t$, respectively.

$$P_{out} = \frac{1}{2} E_{out}^{*} E_{out} \tag{58}$$